

## COMMUNICATION

[View Article Online](#)  
[View Journal](#) | [View Issue](#)Cite this: *RSC Sustainability*, 2025, 3, 3392Received 4th June 2025  
Accepted 4th July 2025

DOI: 10.1039/d5su00406c

[rsc.li/rscsus](https://rsc.li/rscsus)

## Facile hydrothermal synthesis of rare earth hydroxycarbonate phosphors for high-performance warm white LEDs

Haoxuan Zeng,<sup>†a</sup> Qiao Liang,<sup>†a</sup> Lu He,<sup>a</sup> Ziyuan Li,<sup>a</sup> Taihui Chen<sup>ID a</sup>  
and Xiaoli Wu<sup>ID \*abc</sup>

The traditional synthesis of inorganic phosphors often requires complex procedures, including precursor preparation and high-temperature treatment. In contrast, this study introduces a simplified hydrothermal precipitation approach for fabricating europium/terbium hydroxycarbonates ( $\text{Eu}_2(\text{OH})_x(\text{CO}_3)_y(\text{NO}_3)_{(6-x-2y)} \cdot n\text{H}_2\text{O}$  and analogous Tb compound). The synthesized materials demonstrate high thermal stability, with high quenching activation energies ( $E_{\text{a(Eu)}} = 0.283$  eV,  $E_{\text{a(Tb)}} = 0.221$  eV). When applied in white LED devices, these phosphors demonstrate warm white light emission with a color rendering index (CRI) reaching  $R_a = 84.0$  and correlated color temperature (CCT) of 3865 K, making them promising for lighting applications.

## Introduction

Traditionally, rare earth hydroxycarbonates have only been considered as precursors for inorganic phosphors, which typically require subsequent high-temperature treatment to eliminate fluorescence quenching groups or enhance crystallinity to improve luminescence performance.<sup>1,2</sup> On the contrary, during previous studies on YAG films, it was unexpectedly discovered that the hydroxycarbonate precursors of rare earth oxides,<sup>2</sup> particularly europium/terbium hydroxycarbonate, exhibit abnormally strong photoluminescence. The detailed characterization further revealed their high quenching activation energy, making them highly suitable for solid-state lighting applications.

This study develops an optimized hydrothermal synthesis for preparing rare-earth hydroxycarbonates using  $\text{RE}(\text{NO}_3)_3 \cdot 6\text{H}_2\text{O}$  (RE = Eu, Tb) and urea ( $\text{CO}(\text{NH}_2)_2$ ) as raw materials. Compared

## Sustainability spotlight

Hydroxycarbonates synthesized *via* a low-temperature hydrothermal process, while traditionally utilized as rare earth oxide precursors, demonstrate dual functionality as phosphors exhibiting superior thermal quenching resistance and exceptional color rendering properties when employed without subsequent high-temperature annealing, thereby enabling significant energy savings and advancing sustainable material development practices.

with other thermal solvent synthesis methods,<sup>3,4</sup> the hydrothermal synthesis method using only urea is quite simple. In the hydrothermal process, the slow hydrolysis of urea at 100 °C provides controlled  $\text{CO}_3^{2-}$  release kinetics, enabling the growth of monodisperse rare-earth hydroxycarbonates with tunable morphology<sup>5,6</sup> through precise regulation of the  $\text{RE}^{3+}$ : urea molar ratio ( $R = 1 : 3$ ). The resulting phase-pure hydroxycarbonates demonstrate unprecedented thermal stability, maintaining an intensity of >92% at 150 °C, meeting the key requirement of LED phosphors. Notably, the as-prepared rare earth hydroxycarbonate phosphors achieve excellent white light performance (CRI = 84.0, CCT = 3865 K) without requiring the conventional calcination step, showing great potential as phosphor components in white LED devices. This discovery challenges the traditional viewpoint that hydroxycarbonates are only precursors and opens up new possibilities for their direct application in optoelectronic devices.

## Experimental

## Materials

The rare earth metal sources used in the experiments are rare earth nitrates,  $\text{Eu}(\text{NO}_3)_3 \cdot 6\text{H}_2\text{O}$  (99.9% purity) and  $\text{Tb}(\text{NO}_3)_3 \cdot 6\text{H}_2\text{O}$  (99% purity), which were purchased from McLean Biochemicals (Shanghai, China) Co., Ltd. Urea ( $\text{CO}(\text{NH}_2)_2$  99% purity) was purchased from Xi Long Scientific (Guangdong, China) Co., Ltd.

<sup>a</sup>College of Materials Science and Engineering, Guilin University of Technology, Guilin 541004, People's Republic of China<sup>b</sup>Guangxi Key Laboratory of Optical and Electronic Materials and Devices, Guilin University of Technology, Guilin 541004, People's Republic of China<sup>c</sup>Collaborative Innovation Center for Exploration of Nonferrous Metal Deposits, Efficient Utilization of Resources in Guangxi, Guilin University of Technology, Guilin 541004, China. E-mail: wuxiaoli@glut.edu.cn<sup>†</sup> These authors contributed equally to this work.

## Synthesis

For the synthesis of  $\text{RE}_2(\text{OH})_x(\text{CO}_3)_y(\text{NO}_3)_{(6-x-2y)} \cdot n\text{H}_2\text{O}$  (RE = Eu and Tb), the corresponding amount of rare earth nitrates were first dissolved in deionized water to make a 0.05 M rare earth nitrate solution named solution A. Then, urea (the molar ratio of urea to  $\text{RE}^{3+} \approx 3$ ) was added to the above solution A and stirred for 30 minutes to form solution B. Subsequently, the above solution B was hydrothermally treated at 100 °C. After 10 hours, the europium/terbium hydroxycarbonates were obtained through sequential processes of washing, centrifugation, and drying.

## Results and discussion

Under the hydrothermal conditions at 100 °C, urea undergoes the following hydrolysis reaction in Fig. 1(a):  $\text{CO}(\text{NH}_2)_2 + 4\text{H}_2\text{O} \rightarrow \text{CO}_3^{2-} + 2\text{NH}_4^+ + 2\text{OH}^- + 2\text{H}^+$ . The released  $\text{CO}_3^{2-}$  and  $\text{OH}^-$  anions combine with  $\text{RE}^{3+}$  ( $\text{Tb}^{3+}$  and  $\text{Eu}^{3+}$ ),  $\text{NO}_3^-$  and water molecules in the solution to form  $\text{RE}_2(\text{OH})_x(\text{CO}_3)_y(\text{NO}_3)_{(6-x-2y)} \cdot n\text{H}_2\text{O}$  (RE = Tb and Eu). As observed in Fig. 1(b), both XRD patterns exhibit no distinct diffraction peaks except for the background signal, indicating that the Eu/Tb hydroxycarbonates are amorphous.<sup>8</sup> In the FT-IR spectra (Fig. 1(c)), the absorption bands centered at  $689\text{ cm}^{-1}$ ,  $761\text{ cm}^{-1}$ , and  $845\text{ cm}^{-1}$  are attributed to the bending vibrations of C–O bonds, while the peak at  $1086\text{ cm}^{-1}$  originates from the symmetric stretching vibration of  $\text{CO}_3^{2-}$ . The absorption peaks at  $1412\text{ cm}^{-1}$  and  $1516\text{ cm}^{-1}$  correspond to the splitting asymmetric stretching vibrations of  $\text{NO}_3^-$  and  $\text{CO}_3^{2-}$ , respectively.<sup>8</sup> The broad and intense absorption band at  $3408\text{ cm}^{-1}$  is associated with the stretching and bending vibrations of O–H bonds in water molecules, showing strong similarity to previously reported  $\text{Y}_2(\text{OH})_x(\text{CO}_3)_y(\text{NO}_3)_{(6-x-2y)} \cdot n\text{H}_2\text{O}$  compound.<sup>2</sup> SEM images (Fig. 1(d and e)) show that both hydroxycarbonates have a spherical morphology with a wide particle size distribution, and the diameters of the two particles are concentrated within 1  $\mu\text{m}$ . During the initial phase of hydrothermal treatment, temperature variations within the reactor induce differential growth rates among spherical particles. After treatment completion, these particles undergo natural sedimentation, resulting in the observed phenomenon. The EDS elemental mapping confirms uniform elemental distribution without segregation, despite the particle size variations. Notably, nitrogen exhibits a homogeneous but sparse distribution, indicating minimal  $\text{NO}_3^-$  content in the compound structure.

Fig. 2 illustrates the photoluminescence excitation (PLE) and emission (PL) spectra of  $\text{RE}_2(\text{OH})_x(\text{CO}_3)_y(\text{NO}_3)_{(6-x-2y)} \cdot n\text{H}_2\text{O}$  (RE = Eu, Tb). In the PLE spectrum of europium hydroxycarbonate, the excitation peak at 317 nm corresponds to the  ${}^7\text{F}_0 \rightarrow {}^5\text{H}_6$  transition, while peaks at 361 nm, 375 nm, 393 nm, and 415 nm within the 350–450 nm range originate from  $4\text{f}^6$  intra-configurational transitions of  $\text{Eu}^{3+}$  ( ${}^7\text{F}_0 \rightarrow {}^5\text{D}_4$ ,  ${}^7\text{F}_0 \rightarrow {}^5\text{G}_2$ ,  ${}^7\text{F}_0 \rightarrow {}^5\text{L}_6$ , and  ${}^7\text{F}_0 \rightarrow {}^5\text{D}_3$ , respectively<sup>9</sup>), with maximum intensity at 393 nm ( ${}^7\text{F}_0 \rightarrow {}^5\text{L}_6$  transition). Under 393 nm excitation, the PL spectrum exhibits characteristic  ${}^5\text{D}_0 \rightarrow {}^7\text{F}_j$  ( $j = 0, 1, 2, 3, 4$ ) transitions of  $\text{Eu}^{3+}$  at 581 nm, 593 nm, 616 nm, 650 nm, and 701 nm,<sup>10</sup> dominated by the intense red emission at 616 nm

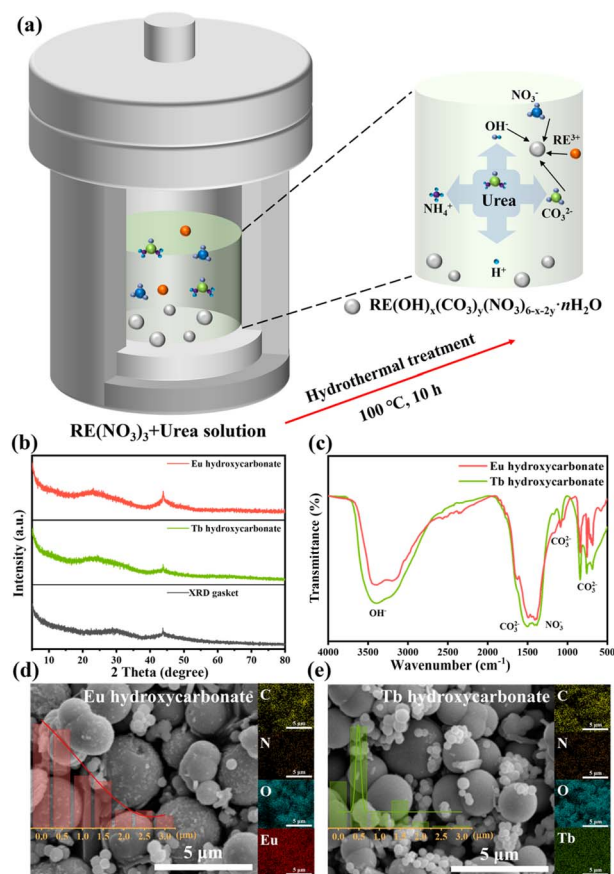


Fig. 1 Formation process of hydroxycarbonate (a), XRD pattern (b), FT-IR spectrum (c), and SEM (EDS) pattern (d and e) of europium/terbium hydroxycarbonate. The illustration in pattern (d and e) is the frequency distribution histogram of two particle sizes.

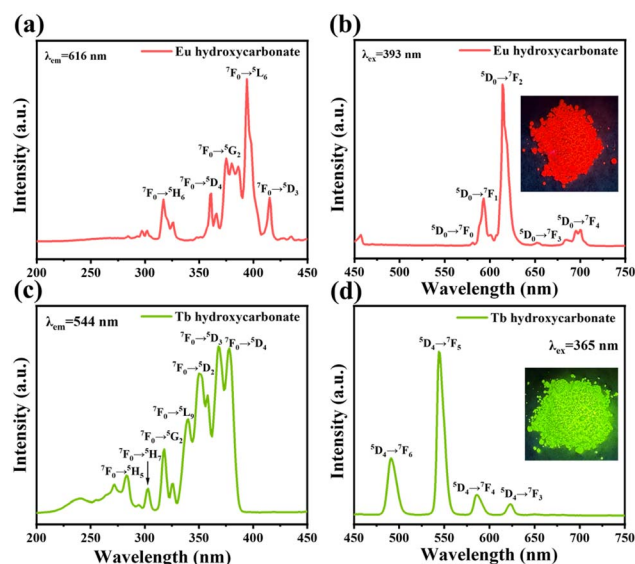


Fig. 2 PLE (a and c) and PL (b and d) spectra of europium/terbium hydroxycarbonate. The insets in (b) and (d) are the actual photographs under the 365 nm excitation for the Tb/Eu hydroxycarbonates, respectively.



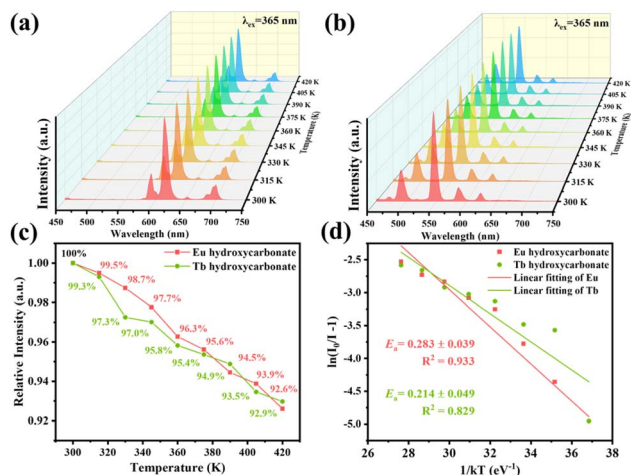


Fig. 3 Temperature-dependent PL spectra (a and b), relative integrated luminescence intensity (c), and thermal quenching activation energy (d) of europium/terbium hydroxycarbonates.

( $^5D_0 \rightarrow ^7F_2$ ). For terbium hydroxycarbonate, the PLE spectrum also shows several peaks between 250–400 nm, excitation peaks at 283, 303, 318, 340, 350, 365, and 378 nm, assigned to  $^7F_0 \rightarrow ^5H_5$ ,  $^7F_0 \rightarrow ^5H_7$ ,  $^7F_0 \rightarrow ^5G_2$ ,  $^7F_0 \rightarrow ^5L_9$ ,  $^7F_0 \rightarrow ^5D_2$ ,  $^7F_0 \rightarrow ^5D_3$ , and  $^7F_0 \rightarrow ^5D_4$  transitions of  $Tb^{3+}$ , respectively.<sup>11</sup> The 365 nm excited PL spectrum displays  $^5D_4 \rightarrow ^7F_j$  ( $j = 6, 5, 4, 3$ ) transitions of  $Tb^{3+}$  at 491 nm, 544 nm, 586 nm, and 623 nm within the 480–650 nm range, with maximum intensity at 544 nm. These two materials emit bright red and green characteristic emissions under the irradiation of 365 nm near ultraviolet lamp, indicating a perfect match with the emission wavelength of the 365 nm near ultraviolet chip.

To assess the application potential of hydroxycarbonates in white LED devices, we systematically studied their thermal stability. The europium/terbium hydroxycarbonate system demonstrates significant thermal quenching suppression abilities, exhibiting exceptional resistance to temperature-induced deactivation. As shown in Fig. 3(a and b), temperature-dependent PL spectra of both phosphors within 300–420 K reveal gradual intensity reductions with increasing temperature while maintaining spectral positions and profiles. Normalized integrated emission intensities relative to the 300 K (room temperature) baseline (Fig. 3(c)) indicates that the hydroxycarbonate phosphors retain over 95% and 93% of their initial intensity at 375 K ( $\sim 100^\circ\text{C}$ ) and 420 K ( $\sim 150^\circ\text{C}$ ), respectively, demonstrating superior thermal stability. To further evaluate the thermal quenching, we calculated the activation energy ( $E_a$ ) using the following Arrhenius equation:<sup>12,13</sup>

$$I_T/I_0 = [1 + c \exp(-E_a/kT)]^{-1} \quad (1)$$

where  $I_0$  and  $I_T$  are the integral area of the emission peaks at 300 K and experimental temperature  $T$ ,  $c$  is a constant, and  $k$  is the Boltzmann constant ( $8.62 \times 10^{-5}$  eV). The relationship between  $\ln(I_0/I_T - 1)$  and  $1/(kT)$  is illustrated in Fig. 3(d). Through fitting calculations, the thermal quenching activation energies ( $E_a$ ) for the hydroxycarbonates were determined to be 0.283 eV and 0.214 eV, respectively. The observed stability arises from a unique synergistic mechanism: the outstanding thermal stability may originate from the synergistic effect of the dynamic coordination network formed by  $RE^{3+}$  with  $OH^-/CO_3^{2-}/NO_3^-$  in the amorphous matrix. This disordered yet compact short-range ordered structure effectively suppresses ion migration at elevated temperatures,<sup>13</sup> thereby preserving the

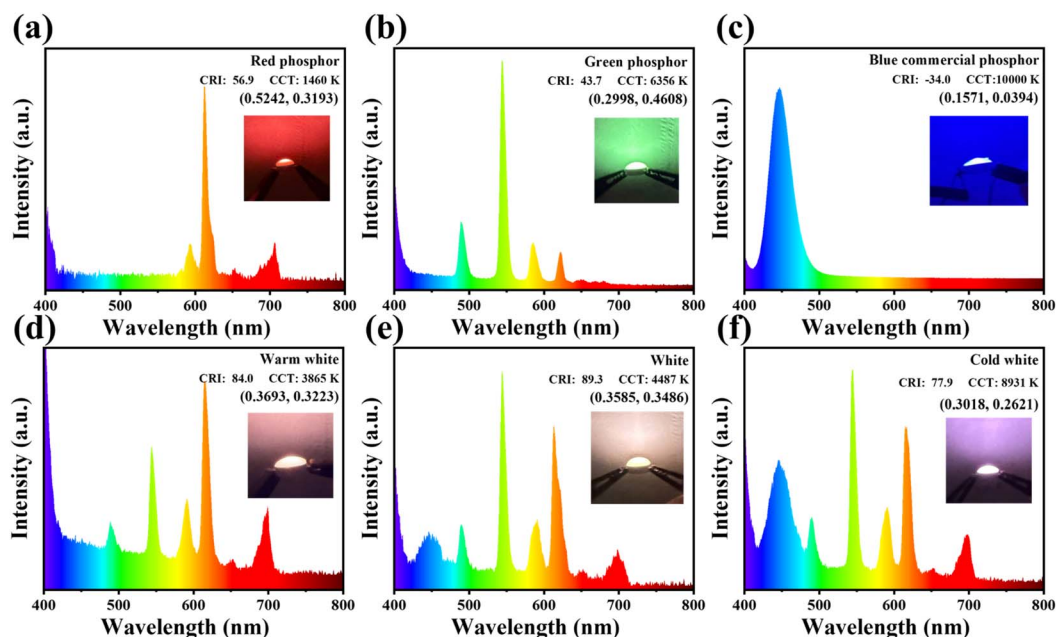


Fig. 4 Photoluminescence spectra of trichromatic phosphors (a–c), binary hydroxycarbonate mixture (d) and with increased blue phosphors trichromatic phosphors (e and f).





coordination environment of  $\text{Eu}^{3+}/\text{Tb}^{3+}$  and significantly reducing non-radiative transition probability.

Higher thermal quenching activation energy values indicate superior thermal stability of the material, meeting the requirements for white LED device fabrication. The aforementioned research results indicate that the excitation wavelength of europium/terbium hydroxycarbonate is highly matched with the wavelength of commercial ultraviolet chips (365 nm), and it has good thermal stability, which provides favorable conditions for its application in white LED.

To modulate white light, it needs to be mixed with commercial blue fluorescent powder ( $\text{Sr}_5(\text{PO}_4)_3\text{Cl}:\text{Eu}^{2+}$ ). In addition,  $\text{Tb}^{3+}$  is easily oxidized to non-emissive  $\text{Tb}^{4+}$  state under high temperature oxidation environment, so it is necessary to use epoxy resin encapsulation technology to inertly protect the hydroxycarbonate system. Fig. 4(a–c) show the photoluminescence spectra of red, green, and blue phosphors cured with epoxy resin under 365 nm ultraviolet LED excitation, respectively, demonstrating the effective excitation of all three phosphors by 365 nm near-ultraviolet light. When combined with commercial blue phosphors, these materials can produce white LED devices with excellent color rendering performance. It is worth noting that commercial blue phosphors ( $\text{Sr}_5(\text{PO}_4)_3\text{Cl}:\text{Eu}^{2+}$ ) produce highly saturated blue emissions (peak at 450 nm), so a low content of blue phosphor is required in the phosphor mixture when modulating white light. Fig. 4(d) shows the warm white light emission achieved through binary hydroxycarbonate mixing, already achieving a CRI of 84. The photoluminescence spectra in Fig. 4(e and f) demonstrate that increasing the blue phosphor content in the tricolor blend system effectively enhances the blue emission component, thereby shifting the overall white light emission from warm white to cool white. The optimized white light obtained a color rendering index of 89.3 and a color temperature of 4487 K. Compared with the warm white light prepared by the pure europium/terbium hydroxycarbonate system, the color rendering and color temperature tunability were significantly improved.

## Conclusions

In summary, this study successfully synthesized and thoroughly characterized two rare earth hydroxycarbonate compounds  $\text{RE}_2(\text{OH})_x(\text{CO}_3)_y(\text{NO}_3)_{(6-x-2y)} \cdot n\text{H}_2\text{O}$ , RE = Eu and Tb, via a hydrothermal method. The synthesis process is straightforward, and the resulting compounds exhibit excellent luminous performance and thermal stability, with thermal quenching activation energies of 0.283 eV and 0.214 eV for europium and terbium hydroxycarbonates, respectively. These materials demonstrate practical utility as phosphor components for white LED applications. The binary hydroxycarbonate achieves high-quality warm white light emission with  $R_a = 84.0$  and CCT = 3865 K. Furthermore, performance enhancement is realized through the combination with commercial blue phosphor,

elevating the white LED device specifications to  $R_a = 89.3$  and CCT = 4487 K.

## Data availability

The authors confirm that the data supporting the findings of this study are available within the article.

## Author contributions

Haoxuan Zeng and Qiao Liang: data curation, investigation, validation, formal analysis and writing original draft. Lu He, Ziyuan Li, and Taihui Chen: formal analysis and methodology. Xiaoli Wu: supervision, funding acquisition, conceptualization, methodology, and writing – review & editing. All authors discussed the results and assisted during manuscript preparation.

## Conflicts of interest

The authors have no conflicts to declare.

## Acknowledgements

The Natural Science Foundation of China (No. 52062011) and Open foundation (Independent Research Project) of Guangxi Key Laboratory of Optical and Electronic Materials and Devices (20AA-6).

## Notes and references

- 1 A. M. Kaczmarek, K. Van Heckeb and R. Van Deun, *Chem. Soc. Rev.*, 2015, **44**, 2032–2059.
- 2 H. X. Zeng, T. H. Chen, Y. P. Guo and X. L. Wu, *Dalton Trans.*, 2025, **54**, 3930–3938.
- 3 Z. Q. Jiang, G. Y. Jiang, D. C. Hou, F. Wang, Z. Zhao and J. Zhang, *CrystEngComm*, 2013, **15**, 315–323.
- 4 B. L. Chen, Y. M. Sun, H. Xiang, M. X. Lin, J. H. Lin and Y. L. Huang, *New J. Chem.*, 2022, **46**, 11021–11024.
- 5 L. Spiridigliozzi, C. Ferone, R. Cioffi, M. Bortolotti and G. Dell'Agli, *Materials*, 2019, **12**, 2062–2079.
- 6 H. J. Zheng, K. J. Zhu, A. Onda and K. Yanagisawa, *Nanomaterials*, 2021, **11**, 529–539.
- 7 T. Litvinova, S. Gerashev, V. Sergeev and E. Lidanovskiy, *Metals*, 2025, **15**, 239–251.
- 8 X. P. Qin, G. H. Zhou, H. Yang, Y. Yang, J. Zhang and S. W. Wang, *J. Alloys Compd.*, 2010, **493**, 672–677.
- 9 H. Y. Chang, F. S. Chen and C. H. Lu, *J. Alloys Compd.*, 2011, **509**, 10014–10019.
- 10 B. Li, R. Shi, Z. Z. Wang, X. Qiao, L. J. Shen and L. Q. Shi, *Colloids Surf., A*, 2024, **698**, 134625.
- 11 J. T. Lin, Y. H. Zheng and Q. M. Wang, *J. Nanopart. Res.*, 2014, **16**, 2552–2565.
- 12 B. B. Yang, J. Zou, F. C. Wang, C. Y. Zhang, J. Y. Xu, L. Li and L. H. Sun, *J. Mater. Sci.: Mater. Electron.*, 2016, **27**, 3376–3383.
- 13 F. Iqbal, S. Kim and H. Kim, *Opt. Mater.*, 2017, **72**, 323–329.

